

# Spin Polarization measurements of $\text{La}_{0.7}\text{Sr}_{0.3}\text{MnO}_3$ (LSMO) single crystals using Point Contact Andreev Reflection Spectroscopy

Maria Viitaniemi

University of Florida, Dept. of Physics, Gainesville, Florida 32612, USA

Amlan Biswas

University of Florida, Dept. of Physics, Gainesville, Florida 32612, USA

Point contact Andreev reflection (PCAR) spectroscopy has received increasing interest as a method for measuring the spin polarization of ferromagnetic materials. We have performed PCAR measurements on aluminum and  $\text{La}_{0.7}\text{Sr}_{0.3}\text{MnO}_3$  (LSMO) single crystals and analyzed the data using various models, including those created by Mazin and Dagehro. Using this information, the various merits and limitations of using PCAR to measure spin polarization are discussed. Measurements performed on unpolarized materials, such as aluminum, produce unreliable results; however, measurements on polarized materials, such as LSMO, show that PCAR has great potential, with additional study, to become a reliable method for the measurement of spin polarization in polarized materials.

## I. Introduction

The accurate measurement of spin polarization in ferromagnetic materials has become increasingly important for use in spintronic devices, such as spin valves and magnetic tunnel junctions.<sup>1-3</sup> Spin polarization ( $P$ ) is a measurement of the imbalance of spin up ( $N_\uparrow$ ) and spin down ( $N_\downarrow$ ) electrons at the Fermi energy ( $E_F$ ) and can be written as<sup>1</sup>:

$$P = (N_\downarrow - N_\uparrow)/(N_\downarrow + N_\uparrow) \quad (1)$$

Currently, the most direct way to measure spin polarization is using point contact Andreev reflection (PCAR) spectroscopy.<sup>4</sup>

PCAR involves creating a nanoscale contact junction between superconducting (S) and normal metal (N) electrodes.<sup>5</sup> An ac voltage is then applied across the junction and the differential conductance ( $dI/dV$ ) is measured. The differential conductance is a measure of the density of states of the electrodes and is a function of the dc voltage ( $V$ ) across the junction;<sup>4</sup>

Therefore,  $dI/dV$  data is acquired as a function of  $V$ . The curves are generally modeled using a theory originally developed by Blonder, Tinkham, and Klapwijk (BTK),<sup>6</sup> which is based on the process of Andreev reflection, a unique phenomenon at the junction of superconductors and metals.<sup>7</sup>

Andreev reflection occurs when a normal metal and a superconductor are brought in direct contact and a voltage is applied across the junction.<sup>1,5</sup> As shown in Fig. 1, if the voltage applied is greater than the energy gap of the superconductor ( $V > \Delta/e$ ), the incident electron will enter the superconductor as a quasiparticle; however, if the voltage applied is less than the gap ( $V < \Delta/e$ ), an electron approaching from the N side will not be able to pass through the contact alone.<sup>1,5</sup> It must form a Cooper pair, which is an up spin and down spin electron couple, and send a hole back into the N side.<sup>1,5</sup> This results in the characteristic doubling of the conductivity of the junction for  $V < \Delta/e$ .<sup>1</sup>

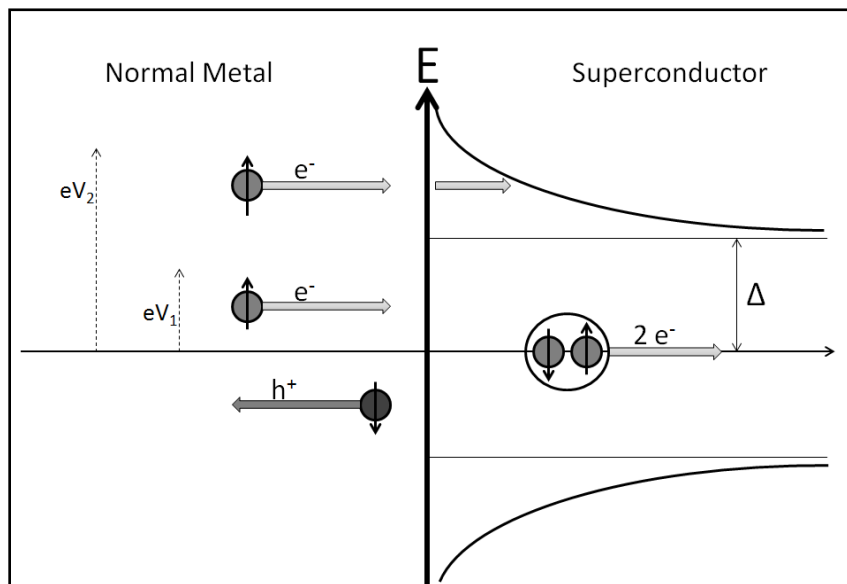


FIG. 1: A N/S junction depicting Andreev reflection. Incident electrons approaching from the left with energies less than the superconducting gap ( $eV_1 < \Delta$ ) must form a cooper pair and reflect a hole in order to pass through the junction. Incident electrons approaching from the left with energies greater than the superconducting gap ( $eV_2 > \Delta$ ) are transmitted as an electron-like quasiparticle. The curves to the right of the junction represent the superconductor's density of states.

To use this method for measuring spin polarization, the normal metal is replaced with the ferromagnet to be characterized.<sup>1,2</sup> Since spin polarized materials have an imbalance of spin up

and spin down electrons, the formation of Cooper pairs, and therefore Andreev reflection, is suppressed or modified.<sup>2,7</sup> This leads to reduced features in  $dI/dV$  vs  $V$  graphs.<sup>4,7</sup>

The original BTK theory only included fitting parameters for gap size ( $\Delta$ ) and barrier transparency,  $Z$ .<sup>5,6,8</sup> Since then a number of models have been developed based on the original BTK theory to include a variety of other parameters like temperature ( $T$ )<sup>5</sup>, angular dependence ( $\theta$ )<sup>5</sup>, lifetime broadening ( $\Gamma$ )<sup>5,9</sup>, as well as spin polarization ( $P$ )<sup>1-4,7,10</sup>. Not all of the new models account for all of the possible parameters.<sup>2,4,7</sup> For example, to our knowledge none of the models for spin polarization include the broadening factor  $\Gamma$ .<sup>2,4,7</sup>

During the course of this project, we have taken spin polarization measurements of aluminum and  $\text{La}_{0.7}\text{Sr}_{0.3}\text{MnO}_3$  (LSMO) single crystals. They are known to be zero<sup>12</sup> and fully spin polarized<sup>11</sup>, respectively, at these temperatures from measurements using various other techniques. Using these data, we describe the various methods we found to best optimize PCAR and provide a discussion of the merits and limitations of using PCAR to measure the spin polarization.

## II. Experimental Methods and Optimization

There are a variety of ways to make ballistic contacts, or junctions where the contact radius is much smaller than the electron mean free path.<sup>5</sup> We have utilized the needle-anvil method,<sup>5</sup> where a sharpened tip is lowered onto a flat sample. The superconducting niobium wire tip was pressed onto the aluminum or LSMO sample surface using a cantilever mechanism. Then using various voltage-generating and -reading instruments the differential of conductance was plotted with respect to voltage.

### A. Tip and Cantilever Fabrication

Niobium tips were made by acid etching<sup>3</sup> 99.9% pure niobium wire, 0.25 mm in diameter. ~2mm of niobium wire was dipped into a 50% potassium hydroxide (KOH) solution along with a carbon rod. The carbon rod and the niobium wire were both attached to an ac variac voltage source and a multimeter. As the voltage was increased to ~4.5-6 Vac, bubbles would appear in the KOH on the surface of the niobium wire. Etching was complete when the bubbling ceased. With continued use, carbon deposits in the KOH solution decreased the effectiveness of the acid etching. To combat this, the voltage was increased incrementally. Additionally, for unknown reasons, as etching progressed the bubbles would become smaller and bubbling less effervescent, indicating slowed etching. Rinsing in water and then replacing into the KOH would often allow etching to continue again at a normal rate. To prevent the formation of KOH crystals on the surface of the niobium wire, the tips were subsequently rinsed in water and ethanol.

The cantilever mechanism, shown in fig. 2, consists of a 1cm long rectangular sheet of phosphor bronze screwed to an L-shaped sample holder. A hypotube, insulated with shrink tube, was embedded in a fitted hole in the rectangular sheet and held in place with Torr Seal epoxy resin (Varian, Inc. Lexington, MA). Tips were cut so that when placed in the hypotube they would almost reach the sample surface before the cantilever was depressed. The hypotube and sample each had two copper wire leads attached to a 4 prong connector.

All measurements were conducted at 4.2K. To achieve this temperature the cantilever was placed at the end of a probe that was then lowered into a helium dewar. The probe had wires attached to a thermometer and heater to measure and control temperature. It also contained a screw on the sample end that could be lowered mechanically to depress the cantilever. Using this mechanism, low resistance,  $<300\Omega$ , contacts were made at room temperature first. As the

apparatus cooled in the dewar the niobium would shrink and the screw mechanism was used to maintain contact and then change the resistance.

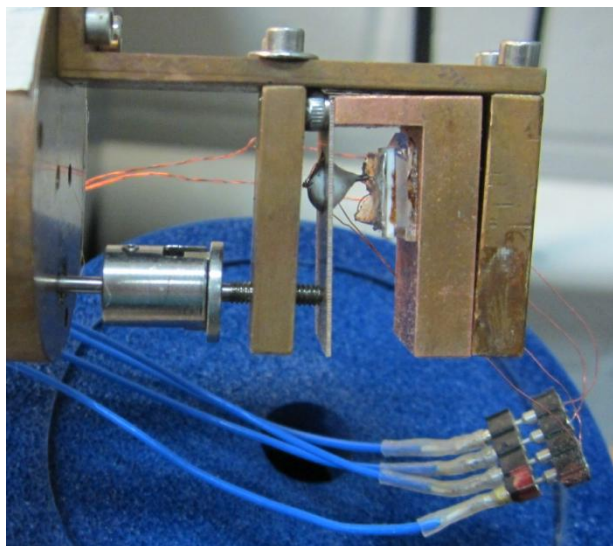


FIG. 2: A phosphor bronze cantilever mechanism inserted into the end of a Helium dewar probe. A niobium tip is in the hypotube attached with Torr Seal resin to the top of the cantilever. The tip is touching an aluminum sample raised on two glass and one sapphire slide. The probe's screw, controlled from the other end of the probe, is slightly depressing the cantilever mechanism. 2 wire leads from the tip and 2 wire leads from the sample (attached behind) attach to the 4 prong connector in the lower right-hand corner.

## B. Experimental Set up and Procedure

We used a lock-in amplifier (Stanford Research Systems, Inc. Sunnyvale, CA) to generate an ac voltage of 4-6 mV(rms) at 70-200 Hz, and a signal generator to produce a slowly varying triangular waveform of 200-300 mV(rms) at 1-2 mHz. These voltages were added and applied across a series combination of the point contact junction and a known resistance of 50-500  $\Omega$ , using a summation circuit that I had previously built and optimized (see fig. 3). The magnitude of the ac and dc (slowly varying triangular waveform) voltages could be further controlled using potentiometers in the circuit. The lock-in amplifier was then used to measure the ac voltage drop across the known resistance ( $R$ ), which when divided by  $R$  provided the value of  $\Delta I$  in the circuit. A Hewlett Packard voltmeter was used to measure the ac voltage drop across the junction which provided the value of  $\Delta V$  across the junction. For small values of  $\Delta V$  the ratio

$\Delta I/\Delta V$  gives us a measure of  $dI/dV$  of the junction. A Labview program<sup>13</sup> plotted  $dI/dV$  vs  $V$ .

Excess noise could be removed and Andreev reflection characteristics enhanced by changing the parameters and magnitude of the ac and dc voltages. The clearest graphs were produced when the voltage drop across the junction was  $\sim 1$  mV.

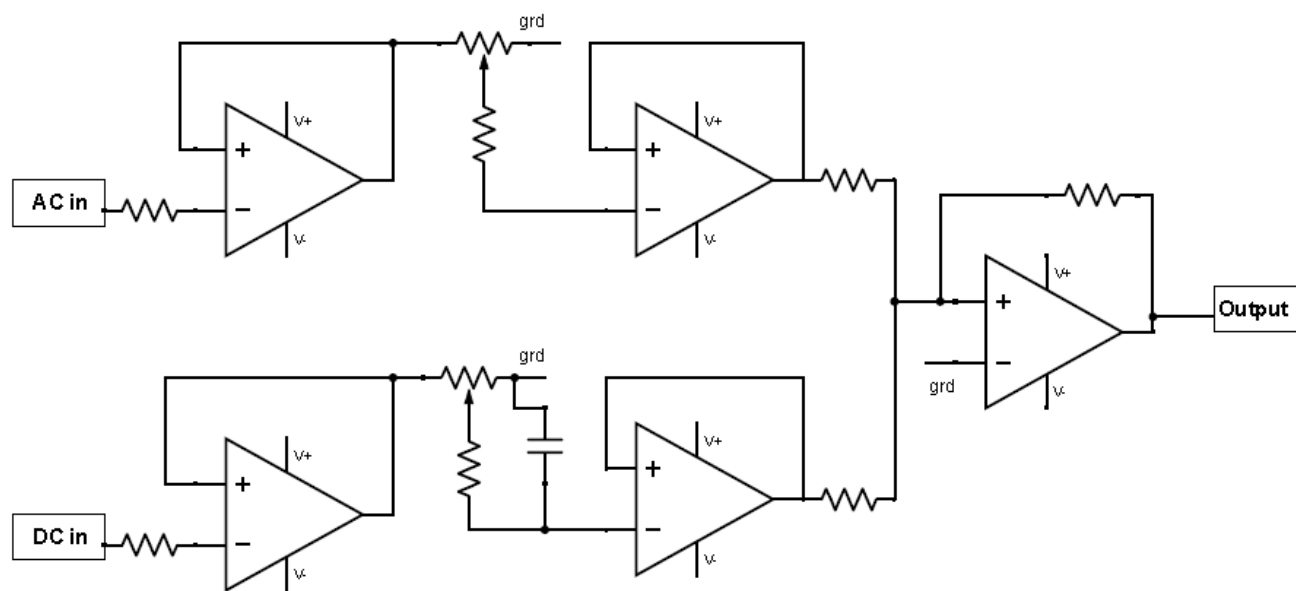


FIG. 3: A circuit diagram of the summation circuit used to combine the AC and DC voltages. Each the AC and the DC voltage comes from a potentiometer and goes through a buffer. They are then combined with an adder (far right). All of the operational amplifiers in this system are OP07s. The output is then sent to a variable resistor over which the voltage drop is measured. It continues to the tip-sample junction and the voltage drop is measured again. These measurements are used in a Labview Program created by John Timmberwilke to generate  $dI/dV$ - $V$  curves.

The cantilever-probe mechanism was used to change the resistance of the junction in the dewar. Changes could be monitored using a multimeter by touching the wires attached to the tip and sample leads. Throughout the process of changing the resistance, the tip often became bent increasing contact radius possibly above the ballistic limit. We are still able to assume a ballistic contact because the oxide layer prevents complete contact and allows only small parallel microjunctions to form.<sup>5</sup> The data we collect is possibly a superposition of many microscopic contacts.

### III. Modeling

Outside the gap region the data began to show features unrelated to Andreev reflection. Therefore, before fitting, this background interference was removed and the data was normalized. Fitting was done using two different models,<sup>5,7</sup> both of which included variables for oxide and other barriers ( $Z$ ), temperature ( $T$ ) and gap size ( $\Delta$ ). A simplified version of a model created by Daghero allows us to account for broadening by scattering events ( $\Gamma$ )<sup>5</sup>. Mazin's formulas include a parameter to account for spin polarization ( $P$ )<sup>7</sup>.

#### A. Normalization

For aluminum, a 2T magnetic field was used to remove the superconductivity of Niobium. This removed all the features of Andreev reflection leaving a V-shaped curve. This curve was divided out of the raw data giving us a flat curve outside of the gap region as predicted by the models. Fig. 4 shows the original data, the background collected at 2T, and the final normalized data.

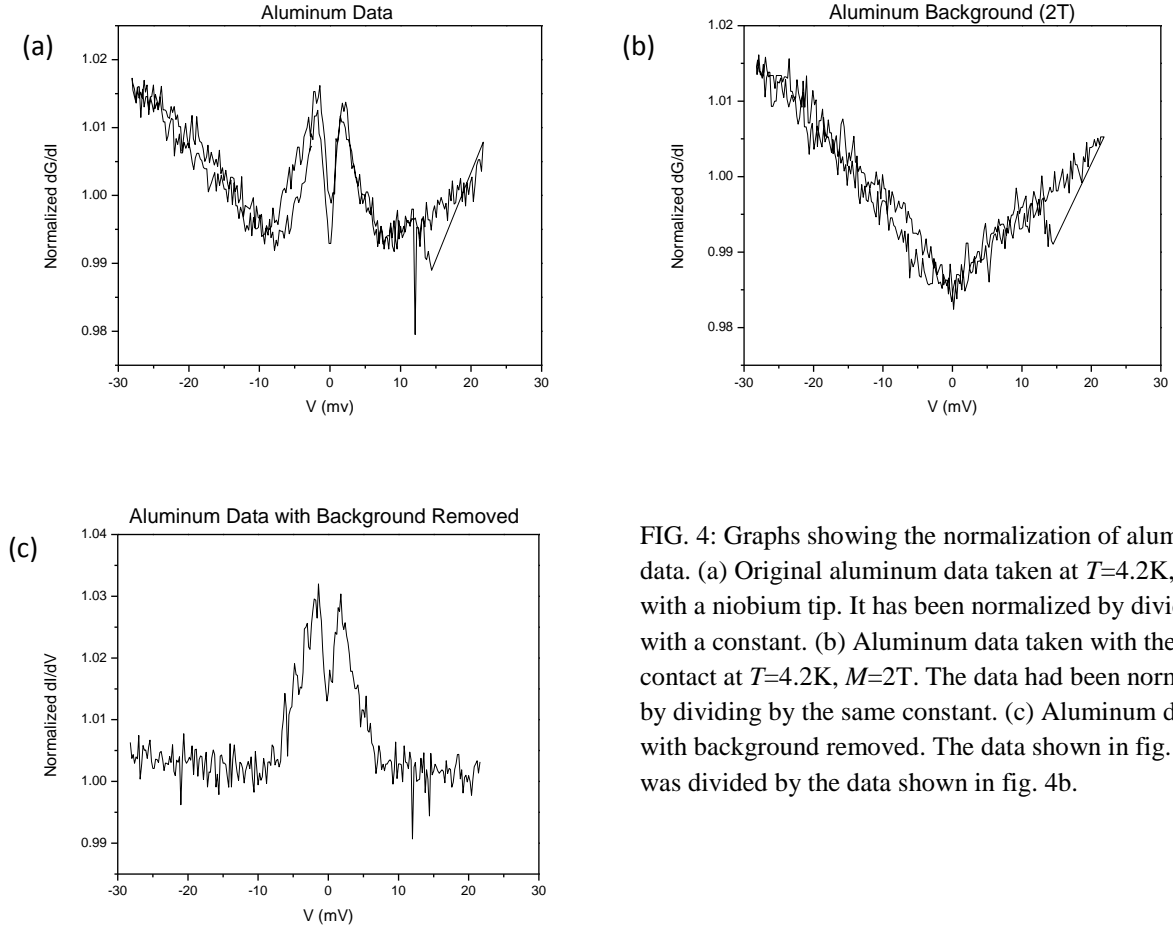


FIG. 4: Graphs showing the normalization of aluminum data. (a) Original aluminum data taken at  $T=4.2\text{K}$ ,  $M=0\text{T}$  with a niobium tip. It has been normalized by dividing with a constant. (b) Aluminum data taken with the same contact at  $T=4.2\text{K}$ ,  $M=2\text{T}$ . The data had been normalized by dividing by the same constant. (c) Aluminum data with background removed. The data shown in fig. 4a was divided by the data shown in fig. 4b.

For LSMO, each of the positive and negative portions of the gap was normalized separately. A linear curve was fit to the data about twice the gap width from the 0V bias then divided out of the raw data. This also left the region outside of the gap flat allowing for fitting.

## B. Broadening by Scattering

Using the method described by Daghero,<sup>5</sup> we began with the original equation for the total current across an N-S junction,

$$I_{NS} = I_0 \int_{-\infty}^{\infty} [f(E - eV) - f(E)][1 + A(E) - B(E)]dE \quad (2)$$

where  $f(E)$  is the Fermi distribution function,  $A(E)$  is the probability of Andreev reflection,  $B(E)$  is the probability of ordinary reflection, and the quantity  $[1+A(E)-B(E)]$  is the transmission probability.<sup>14</sup> The transmission probability can also be represented by

$$\sigma(E) = \tau_N \cdot \frac{1 + \tau_N |\gamma(E)|^2 + (\tau_N - 1) |\gamma(E)^2|^2}{|1 + (\tau_N - 1) \gamma(E)^2|^2} \quad (3)$$

where

$$\tau_N = \frac{1}{1 + Z^2} \quad (4)$$

and

$$\gamma(E) = \frac{E - \sqrt{E^2 - \Delta^2}}{\Delta} \quad (5)$$

$E$  is the energy over which we integrate,  $\Delta$  is the gap size of the superconductor, and  $Z$  is the barrier transparency.

By using the Fermi function at a finite  $T$  ( $f(E, T)$ ), and taking the derivative with respect to the bias voltage, a formula for the differential of conductance at a finite temperature emerges:

$$\frac{dI_{NS}}{dV}(V) = I_0 \frac{d}{dV} \int_{-\infty}^{\infty} [f(E - eV, T) - f(E, T)] \sigma(E) dE \quad (6)$$

To include a parameter to account for broadening by scattering events ( $\Gamma$ ), the imaginary part of energy is included in  $\sigma(E)$ , so

$$E \rightarrow E + i\Gamma \quad (7)$$

Fig. 5a shows how  $\Gamma$  causes the broadening of the Andreev reflection features.

### C. Spin Polarization

To fit the data for spin polarization, models for the differential of conductance curve with respect to voltage for fully polarized material ( $G_P(V)$ ) and for a fully unpolarized material ( $G_N(V)$ ) were added together in a ratio determined by  $P^2$ :

$$G(V) = (1 - P)G_N(V) + PG_P(V) \quad (8)$$

There are a number of different sources for  $G_N(V)$  and  $G_P(V)$ .<sup>2</sup> We found Mazin's method to provide the best fit.<sup>7</sup> It is summarized in Table 1. This method does not include  $\Gamma$ , but  $\Gamma$  can be roughly simulated by increasing temperature (see fig. 5).

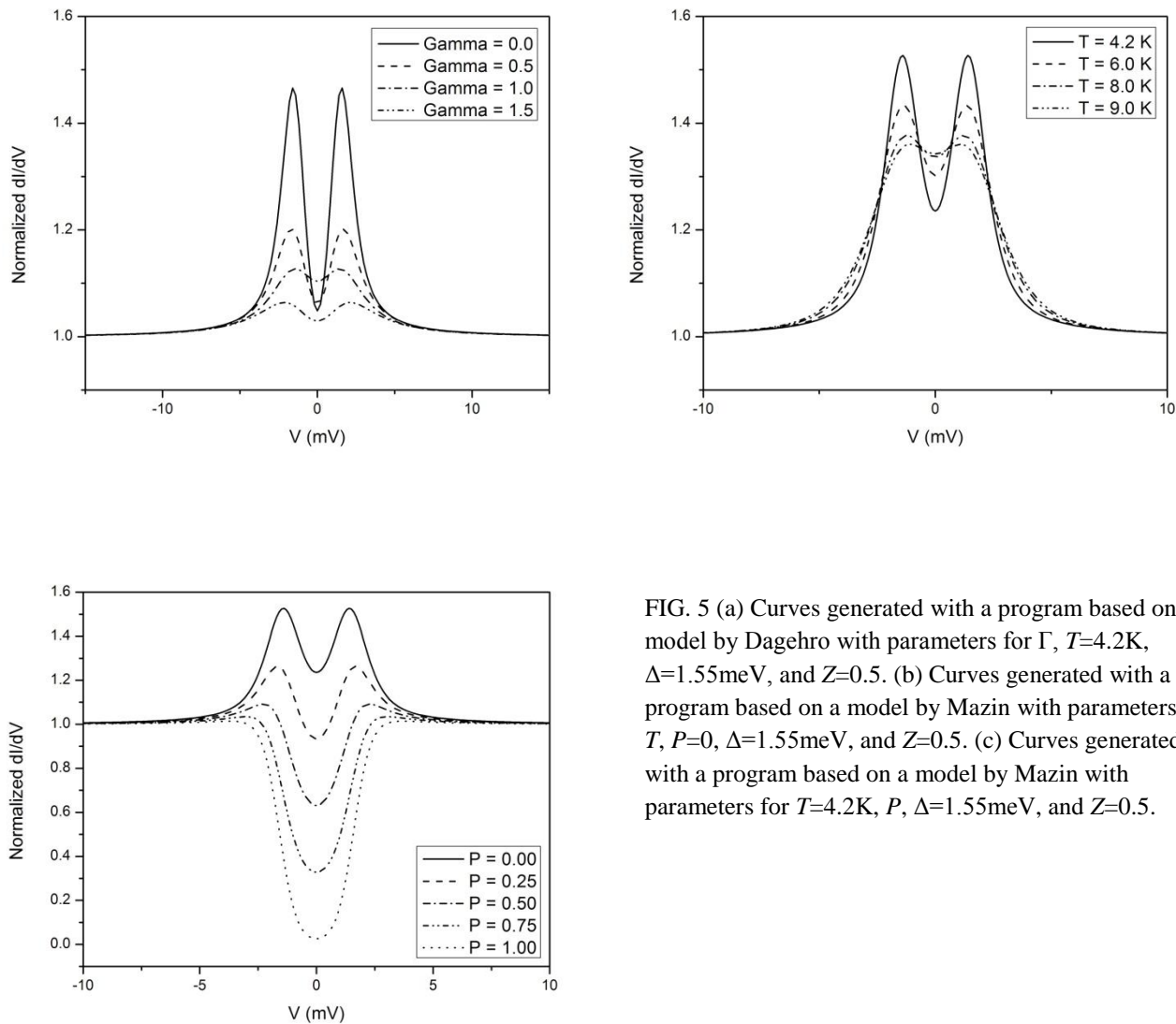


FIG. 5 (a) Curves generated with a program based on a model by Dagehro with parameters for  $\Gamma$ ,  $T=4.2$ K,  $\Delta=1.55$ meV, and  $Z=0.5$ . (b) Curves generated with a program based on a model by Mazin with parameters for  $T$ ,  $P=0$ ,  $\Delta=1.55$ meV, and  $Z=0.5$ . (c) Curves generated with a program based on a model by Mazin with parameters for  $T=4.2$ K,  $P$ ,  $\Delta=1.55$ meV, and  $Z=0.5$ .

TABLE I. Formulas for the conductance of a fully unpolarized material  $G_N(V)$  and a fully polarized material  $G_P(V)$  at  $T=0$  and  $\beta = E / \left( \sqrt{|\Delta^2 - E^2|} \right)$  by Mazin. As  $T \rightarrow 0$ , the Fermi-Dirac distribution function approaches a  $\delta$  function which is why it is not included as in formula 6.

	$ E  < \Delta$	$ E  > \Delta$
$G_N(E) = 1 + A_N - B_N$	$\frac{2(1 + \beta^2)}{\beta^2 + (1 + 2Z^2)^2}$	$\frac{2\beta}{1 + \beta + 2Z^2}$
$G_P(E) = 1 + A_P - B_P$	0	$\frac{4\beta}{(1 + \beta)^2 + 4Z^2}$

## IV. Results and Discussion

### A. Aluminum

We first tested aluminum, an unpolarized material,<sup>12</sup> to confirm that our apparatus was working properly.  $T$  was set to 4.2K. The values for  $Z$  and  $\Gamma$  were reasonable viz. 0.5 - 0.7 and 1.3 - 1.6 meV respectively.  $\Delta$  for niobium is known to be 1.55 meV, but better fits were achieved when  $\Delta$  was allowed to change. The reduction in  $\Delta$  can be accounted for by the proximity effect<sup>15</sup> that occurs in N/S junctions. All of the values are near what we expected, confirming that our methods were correct.

However, fitting with  $P$  gave unexpected results. The best fits found aluminum to be spin polarized with  $P$  between 0.395 and 0.495 (see figure 6). Even when we increased temperature to account for gamma, it was not possible to fit without accounting for some  $P$  above 0. In previous literature,<sup>10</sup> similar problems have been shown when using PCAR to measure spin polarization in other materials that are known to not be spin polarized. The PCAR method does not seem to be effective at measuring  $P$  for materials with low spin polarization values.

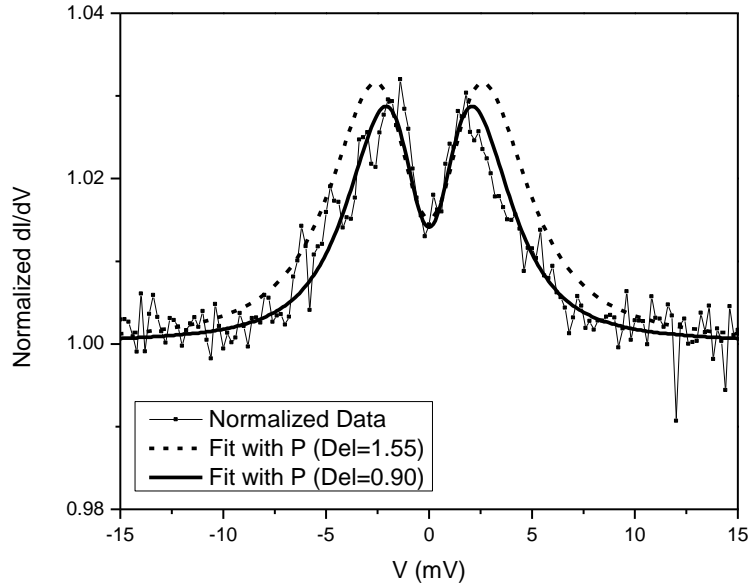


FIG. 6: Aluminum and Niobium PCAR data taken at 4.2K. Fitting was done with a program based off a model by Mazin. The solid line is a fit where  $\Delta$  was allowed to vary. When  $\Delta=0.9\text{meV}$ ,  $P=0.495$ ,  $Z=0.435$ , and  $T=12$ . The dashed line shows when  $\Delta=1.55\text{meV}$ ,  $P=0.405$ ,  $Z=0.120$ , and  $T=12$ . Aluminum is not spin polarized, but it was impossible to fit the data with  $P=0$ .

## B. LSMO

The magnetic properties of LSMO have been studied in great detail using a number of different methods;<sup>11</sup> therefore it is known to be at least partially spin polarized at the surface. For this reason we only used the model including spin polarization to fit the data.

Unexpectedly, the gap appeared much larger than the known value of 1.55 meV for niobium wire. This may be the result of the series resistance caused by the method used to attach the leads to the LSMO sample. By reducing the gap size of the data mathematically by 50-70%, we were able to reasonably fit the data. Better methods of attaching the sample wires or of accounting this series resistance are important for further development of PCAR.

Once the gap size was reduced, LSMO was found to be ~50% spin polarized at the surface. The fits were consistent over a number of junctions with values of  $P$  ranging from 0.495-0.500 (see Table 2). We are confident in these values of  $P$ , because as shown in figure 7,

very minute changes in  $P$  values result in drastic changes in the shape of the curve. For this reason, PCAR shows promise as a reliable method for the determination of spin polarization, but only after more optimization and study.

Table 2: A table of the values used to fit a number of sets of PCAR data. Data was taken with an LSMO sample and niobium tip at 4.2K. Temperature ( $T$ ) was allowed to vary to simulate a changing  $\Gamma$ . Percent indicates the percent with which the gap size was reduced. Notice that the values of  $P$  are very consistent.

Fit Number	$\Delta$	$Z$	$P$	$T$	Percent
1	1.55	0.070	0.500	5.5	0.60
2	1.55	0.080	0.500	6.0	0.55
3	1.55	0.110	0.500	7.0	0.58
4	1.55	0.130	0.495	5.0	0.50
5	1.55	0.143	0.497	5.4	0.55
6	1.55	0.185	0.500	9.0	0.70
7	1.55	0.190	0.500	9.0	0.70

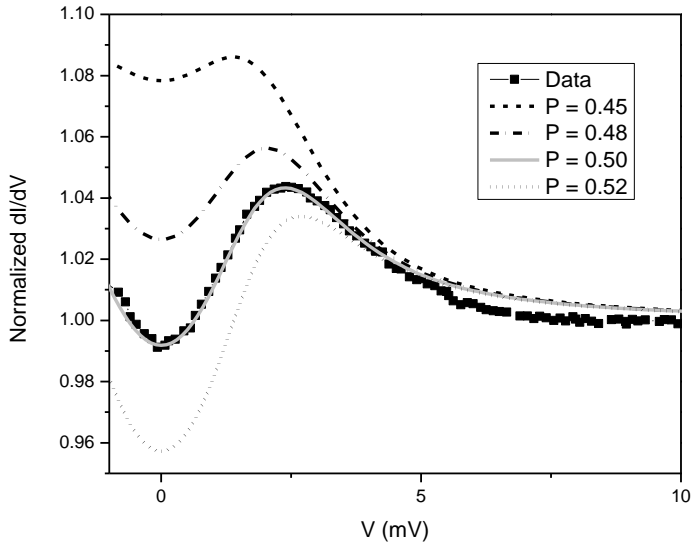


FIG. 7: A graph showing the data and fit for a PCAR measurement with an LSMO sample and niobium tip at 4.2K. It is fit number 2 on Table 2. Also shown are fits with different values of  $P$  with all else held constant.

There was also often some level of ambiguity in the range of data to use for the removal of background function, because outside the bias the background quickly becomes nonlinear. We found that small differences in the data used for background removal lead to changes in the

shape of the graphs. This resulted in noticeably different values for all of the fitting parameters or an inability to fit graphs at all. In order to find more reliable spin polarization measurements a better method must be determined to remove background noise.

It is also interesting to note that the first measurements we took did not show any Andreev reflection. Features only appeared when we got a new crystal. This is most likely because the original crystal had been used for many experiments previously and had a contaminated surface. This observation shows that sample quality is very important for PCAR.

## **V. Conclusions**

PCAR does not seem to be a reliable method for the measurement of spin polarization in unpolarized materials such as aluminum.  $P$  in these materials should be very near 0, but the best fits were found to be much higher, around 0.40. However, in measuring spin polarization in polarized materials, PCAR shows great promise after more study and optimization have been done. Our tests showed consistency over a number of trials though more tests with different materials would be needed to confirm this consistency. Other issues with PCAR that need to be better understood include: (1) how to properly normalize and remove background from data; (2) how to model for both  $\Gamma$  and  $P$  in the same program; (3) how to determine the series resistance in sample connections; and (4) how to determine the quality of a sample.

## ACKNOWLEDGEMENTS

This work was supported by the UF Materials Physics REU Program through NSF grant DMR-1156737. The author would like to thank all members of the Biswas Lab, especially J. Timmerwilke for assistance and advice throughout much of the work as well as for allowing the use of his programs as learning tools. Thanks is also given to everyone who assisted with the University of Florida REU program.

<sup>1</sup> P. Chalsani, S. K. Upadhyay, O. Ozatay, and R. A. Buhrman, Phys. Rev. B **75**, 094417 (2007).

<sup>2</sup> Y. Ji, G. J. Strijkers, F. Y. Yang, and C. L. Chien, Phys. Rev. B **64**, 224425 (2001).

<sup>3</sup> Everett Grimley, "Implementation of Point-Contact Andreev Reflection and the Modified BTK Model for Determining Spin-Polarization of Ferromagnetic Crystals and Thin Films," (2012).

<sup>4</sup> G. J. Strijkers, Y. Ji, F. Y. Yang, and C. L. Chien, Phys. Rev. B **63**, 104510 (2001).

<sup>5</sup> D. Daghero and R. S. Gonnelli, Supercond. Sci. Technol., **23**, 043001 (2009).

<sup>6</sup> G. E. Blonder, M. Tinkham and T. M. Klapwijk, Phys. Rev. B **25**, 4515 (1982).

<sup>7</sup> I. I. Mazin, A. A. Golubov and B. Nadgorny, Journal of App. Phys. **89**, 7576 (2001).

<sup>8</sup> Z was originally used to account for the oxide layer in a point contact; however, it is now recognized to also account for other factors that contribute to electron scattering such as poor contact and bending of the tip.<sup>5</sup>

<sup>9</sup> The broadening of gap features is a result of the reduction of the quasiparticle lifetime.

<sup>10</sup> Y. Bugoslavsky, Y. Miyoshi, S. K. Clowes, W. R. Branford, M. Lake, I. Brown, A. D. Caplin, and L. F. Cohen, Phys. Rev. B **71**, 104523 (2005).

<sup>11</sup> J. -H Park *et al.*, Phys. Rev. Lett. **81**, 1953 (1998).

<sup>12</sup> J. F. Cochran and D. E. Mapother, Phys. Rev. Lett. **111**, 132 (1958).

<sup>13</sup> Lview program by J. Timmerwilke, University of Florida.

<sup>14</sup> Although not noted, the contributions of  $C(E)$  and  $D(E)$  have also been taken into account.  $C(E)$  is the probability of the transmission of an oncoming electron in S as an electronlike quasiparticle.  $D(E)$  is the probability of transmission of an oncoming electron with Fermi-Surface crossing.<sup>5</sup>

<sup>15</sup> The proximity effect is an effect where on the normal metal side of an N/S junction near the contact the normal metal begins to act as a superconductor. This results in reduced gap size.